Steel and Composite Structures, *Vol. 34, No. 6* (*2020*) *803-818*
DOI: https://doi.org/10.12989/scs.2020.34.6.803

Modelling and experiment of semi rigid joint between composite beam and square CFDST column

Lei Guo[1], Jingfeng Wang*[1,2] and Meng Zhang[1]

[1]*School of Civil Engineering, Hefei University of Technology, Tunxi Road 193, Anhui Province, 230009, China*
[2]*Anhui Civil Engineering Structures and Materials Laboratory, Tunxi Road 193, Anhui Province, 230009, China*

(*Received September 16, 2019, Revised January 16, 2020, Accepted February 20, 2020*)

Abstract. Semi-rigid connections with blind bolts could solve the difficulty that traditional high strength bolts were unavailable to splice a steel/composite beam to a closed section column. However, insufficient investigations have focused on the performance of semi-rigid connection to square concrete filled double-skin steel tubular (CFDST) columns. In this paper, a component model was developed to evaluate the mechanical behavior of semi-rigid composite connections to CFDST columns considering the stiffness and strength of column face in compression and column web in shear which were determined by the load transfer mechanism and superstition method. Then, experimental investigations on blind bolted composite joints to square CFDST columns were conducted to validate the accuracy of the component model. Dominant failure modes of the connections were analyzed and this type of joint behaved semi-rigid manner. More importantly, strain responses of CFDST column web and tubes verified that stiffness and strength of column face in compression and column web in shear significantly affected the connection mechanical behavior owing to the hollow part of the cross-section for CFDST column. The experimental and analytical results showed that the CFDST column to steel-concrete composite beam semi-rigid joints could be employed for the assembled structures in high intensity seismic regions.

Keywords: square concrete-filled double skin steel tubular (CFDST); composite beam; semi-rigid; component model

1. Introduction

Concrete-filled double skin steel tubular (CFDST) column is composed of inner and outer steel tubes placed concentrically and infilled concrete, as shown in Fig. 1. It is inherited from the concrete filled steel tube (CFST) by replacing a portion of core concrete with steel tube, which significantly reduces the self-weight and improves the bending stiffness and strength as well. As a result, the CFDST column has broad application prospects in engineering practice especially in high rise and large-span buildings.

Presently abundant researches were carried out on CFDST members by Wei *et al*. (1995), Han *et al*. (2004), Huang *et al*. (2013), Zhou and Xu (2016) and Farahi *et al*. (2016), confirming that the CFDST columns behaved excellent structural performance. However, insufficient investigations have focused on the performance of CFDST column joints. Chen *et al*. (2016) and Hou and Han (2017) only studied welded joints to CFDST columns. For a beam to CFDST column joint in frame structures, traditional high strength bolts were inconvenient to be employed. To overcome this difficulty, various blind fasteners including Hollo-bolt, One-side, Flowdrill, and Huck fasteners (Mirza and Brain 2011) are developed. Up until now, there are some investigations focusing on the beam to CFDST column semi-rigid connections using blind bolts (Guo *et al*. 2019 a, b, Wang *et al*. 2019). These experimental results declared that the semi-rigid connections with CFDST columns performed excellent seismic behavior. At the same time, connecting a CFDST column and a beam using blind bolts could eliminate the fielding weld work and could accelerate the construction speed as well.

Mechanical behavior of each connection could be estimated by the component method introduced in EC3 (2005). Currently, component models for blind bolted joints of CFST column have already been systematically established (Agheshlui *et al*. 2017, Theodoros and Walid 2015). Although some existed researches extended the analytical model to predict the mechanical behavior of semi-rigid connection to CFDST column (Guo *et al*. 2019 a, b, Wang *et al*. 2019). These analytical models mainly focused on the semi-rigid connection to circular CFDST column and ignored the stiffness coefficients of the CFDST column. Only Wang *et al*. (2019) proposed an equivalent method to estimate the initial stiffness of semi-rigid connection between the square CFDST column and the steel beam without meticulously considering the feature of square CFDST column. To promote the application of CFDST structures, it is essential to establish a well thought out component model to accurately simulate the mechanical performance of semi-rigid composite connection to square CFDST column.

*Corresponding author, Professor
E-mail: jfwang008@163.com

ISSN: 1229-9367 (Print), 1598-6233 (Online)

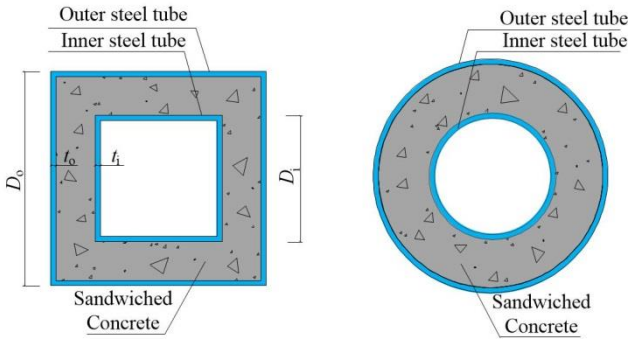

Fig. 1 Typical cross sections of CFDST columns

Therefore, this paper developed a component model for analyzing the initial stiffness and moment resistance of semi-rigid connection between the composite beam and square CFDST column. To determine the stiffness and strength coefficients of CFDST column wall and web, load transfer mechanism of the blind bolt in tension and beam flange in compression were discussed. Following this, an experimental investigation on semi-rigid composite joints to square CFDST columns with flush or extended end plates was carried out to validate the proposed component model. Strain responses of the CFDST column web and tube were discussed in detail to inspect their stress states. Dominant failure modes of this type of connection were also presented. In addition, seismic performance of the connection between the square CFDST column and composite beam was also discussed. The observed component model and experimental results were beneficial for the construction and design of composite structures in engineering practice.

2. Component model

For semi-rigid connections to CFDST columns using blind bolts, the blind bolt is inserted across the double steel tubes and the sandwiched concrete. Therefore, the inner and outer tubes associated with the sandwiched concrete work together to restrict local buckling of the column tube, which also significantly increases the stiffness of column tube in tension. Therefore, the stiffness of column face in tension is significantly greater than those of end plate in bending and bolt in tension, so it is assumed reasonable to ignore the column face in tension in the component model. However, the hollow part of the section deteriorates the stiffness and strength of column face in compression ($K_{cf,c}$) and column web in shear ($K_{cw,s}$). Existing analytical investigations have not considered the stiffness and strength of $K_{cf,c}$ and $K_{cw,v}$ in the component model for the semi-rigid composite connection to square CFDST column. Guo *et al*. (2019b) has proposed a component model which is proper for the semi-rigid composite connection to CFDST column considering the partial shear behavior. The predicted moment resistance coincides well with the experimental results, while at the same time the proposed model overestimates the initial stiffness of the semi-rigid connections probably because the stiffness of $K_{cf,c}$ and $K_{cw,s}$ are not taken into consideration.

As discussed above, a component model is developed to calculate the initial stiffness and moment resistance of the semi-rigid connection, in which the stiffness and strength of $K_{cf,c}$ and $K_{cw,s}$ are both incorporated.

2.1 Initial stiffness

2.1.1 Joint under hogging moment

As presented in Fig. 2, the initial stiffness of the joint under hogging moment is calculated as

$$S_{j,ini,h} = \frac{z_{eq}^2}{1/K_{cf,c} + 1/K_{cw,s} + 1/K_{eq}} \tag{1}$$

$$K_{eq} = \frac{(K_{eq,r} z_{eq,r} + \sum_i K_{eq,i} z_i)^2}{K_{eq,r} z_{eq,r}^2 + \sum_i K_{eq,i} z_i^2} \tag{2}$$

$$z_{eq} = \frac{K_{eq,r} z_{eq,r}^2 + \sum_i K_{eq,i} z_i^2}{K_{eq,r} z_{eq,r} + \sum_i K_{eq,i} z_i} \tag{3}$$

$$K_{eq,i} = \frac{1}{1/K_{bo,i} + 1/K_{ep,i}} \tag{4}$$

$$K_{eq,r} = \frac{1}{\frac{1}{K_{ur} + K_{1r}} + \frac{1}{K_{sc}}} \tag{5}$$

$$z_{eq,r} = \frac{K_{ur} z_{ur}^2 + K_{1r} z_{lr}^2}{K_{ur} z_{ur} + K_{1r} z_{ur}} \tag{6}$$

in which K_{ur} and K_{lr} denote the upper and lower layers of reinforcement in tension calculated by CEB-FIP Model Code (1990), respectively; $K_{bo,i}$ and K_{ep} are the ith bolt row in tension and end plate in bending introduced in EC3 (2005), respectively; K_{sc} is the stiffness of shear connector observed by Aribert (1996) and expressed by

$$K_{sc} = \frac{N_h k_{sc}}{\beta - \frac{\beta - 1}{1 + \alpha} \frac{z_r}{d_r}} \tag{7}$$

$$\alpha = \frac{EI}{E_r A_r d_r^2} \tag{8}$$

$$\beta = \sqrt{\frac{(1+\alpha) N_h k_{sc} l_s d_r^2}{EI}} \tag{9}$$

where N_h and is the number of shear connector distributed in the hogging moment;. k_{sc} is the elastic stiffness of the shear connector. d_r is the distance between the reinforcement and the centerline of the steel beam.

In order to calculate $K_{cf,c}$ for CFDST column, the load transfer mechanism from the outer tube to the sandwiched concrete and to inner tube should be primarily clarified. As illustrated in Fig. 3, the compressive force dispersed at the slope of 1:1 within the sandwiched concrete from the outer tube to the inner tube (Yang *et al*. 2015). Moreover, the double steel tubes and sandwiched concrete work together without separation, so that $K_{cf,c}$ is expressed by

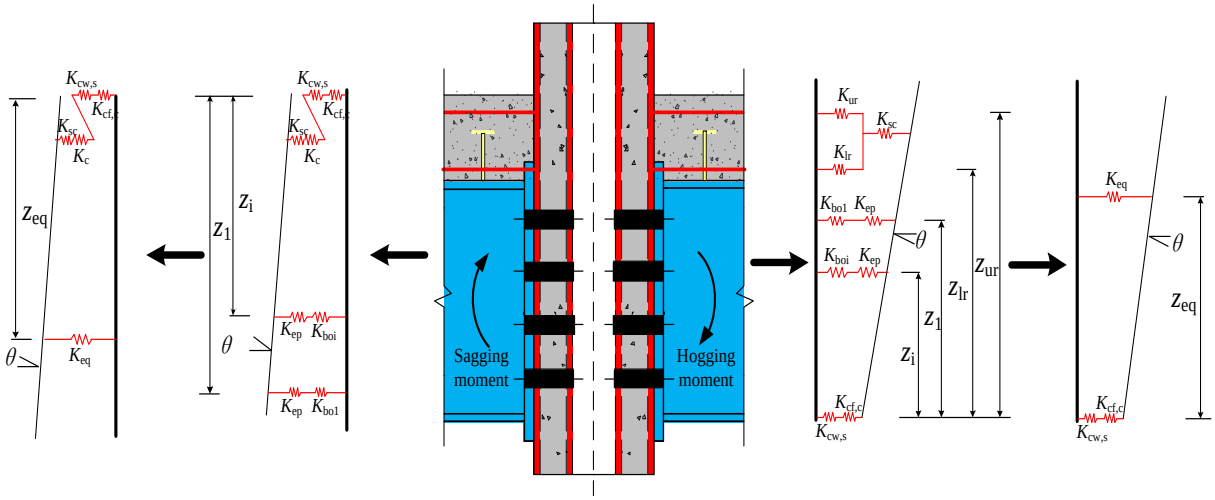

(I) Sagging moment (II) Hogging moment

(a) Flush end plate connection

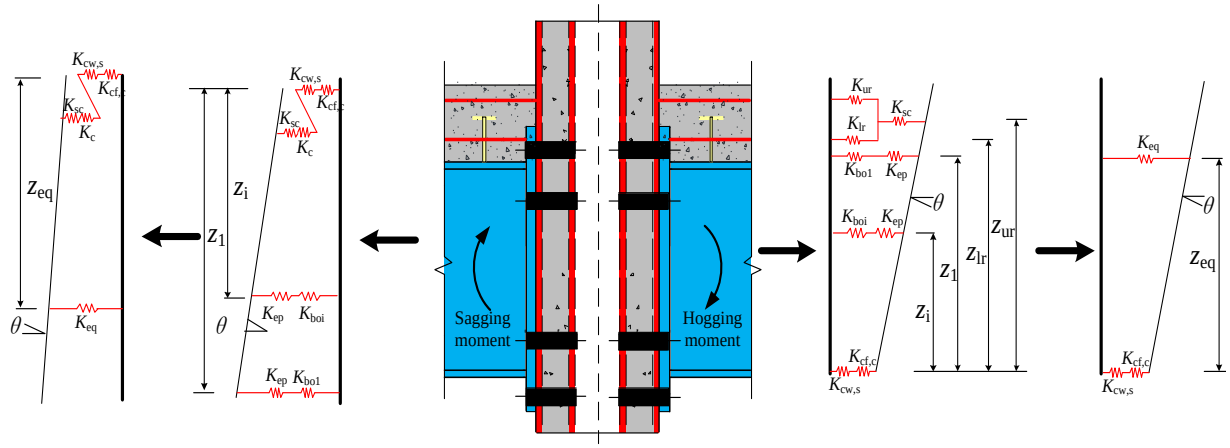

(I) Sagging moment (II) Hogging moment

(b) Extended end plate connection

Fig. 2 Component models to calculate the initial stiffness of the connections

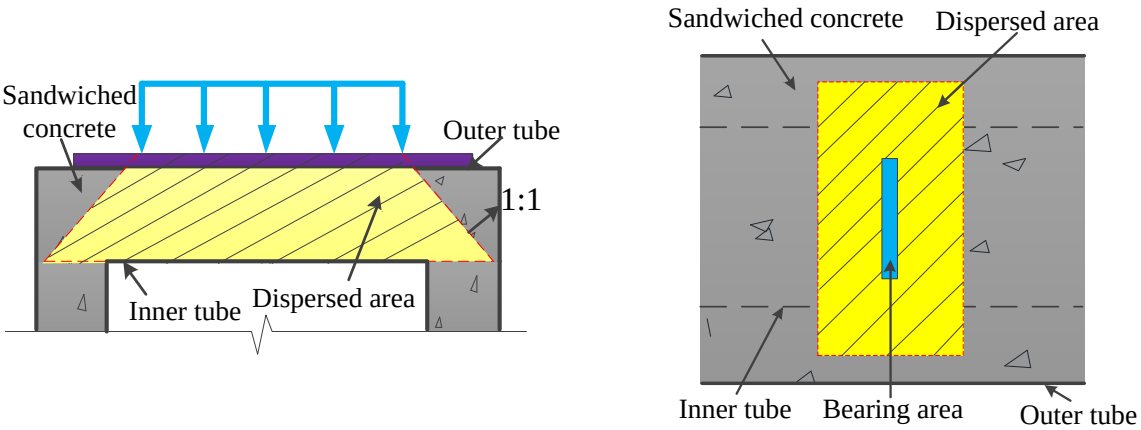

(a) Side view (b) Longitudinal view

Fig. 3 Load transfer mechanism for blind bolted connections to CFDST columns

$$K_{cf,c} = K_{o,c} + K_{s,c} + K_{i,c} \tag{10}$$

in which $K_{o,c}$ and $K_{i,c}$ are the outer and inner tube in compression, respectively, and are expressed by Liu *et al*. (2012)

$$K_{o,c} or K_{i,c} = \frac{2\pi E t^3}{3(1-\nu^2)C_t(b\text{-}t)^2} \tag{11}$$

$$C_t = 0.3In(b/c)+0.03 \tag{12}$$

hereinto, v is the Poisson ratio; b and t are the width and thickness of steel tube, respectively; c is the width of compressive area for the steel tube.

$K_{s,c}$ denotes the sandwiched concrete in compression and is calculated based on the load transfer mechanism

$$K_{s,c} = \frac{4E_c(b_f - t_f)}{In\frac{t_f+(1\text{-}\chi)(D_o\text{-}2t_o)}{A} - In\frac{t_f}{b_f}} \tag{13}$$

where

$$A = \min\begin{cases} b_f + (1-\chi)(D_o - 2t_o) \\ D_o \end{cases} \tag{14}$$

Different from the CFST column, the web of CFDST column consisted two steel plates and infilled concrete. In the initial stage, $K_{cw,s}$ is estimated based on the superstition method

$$K_{cw,s} = K_{o,s} + K_{s,s} + K_{i,s} \tag{15}$$

in which $K_{o,s}$, $K_{s,s}$ and $K_{i,s}$ are the shear stiffness contributed by the outer tube, sandwiched concrete and inner tube, respectively. According to EC3 (2005) and Du *et al*. (2005), $K_{o,s}$, $K_{s,s}$ and $K_{i,s}$ are achieved by

$$K_{w,s} = \frac{0.38E_sA_{vc}}{\beta z} \tag{16}$$

$$K_{s,s} = A_c G_c / 1.2h_j \tag{17}$$

hereinto, G_c is the shear modulus of sandwiched concrete; β and z are the transmission parameter and lever arm, respectively. A_t and A_c are the shear areas of column tube and sandwiched concrete, respectively. h_j is the height of joint core.

2.1.2 Joint under sagging moment

The component model for evaluating the initial stiffness of the connection under sagging moment is displayed in Fig. 2. Following equations are employed to evaluate the initial stiffness

$$S_{j,ini,h} = \frac{z_{eq}^2}{1/K_{eq,c} + 1/K_{eq}} \tag{18}$$

$$K_{eq} = \frac{(\sum_i K_{eq,i}z_i)^2}{\sum_i K_{eq,i}z_i^2} \tag{19}$$

$$z_{eq} = \frac{\sum_i K_{eq,i}z_i^2}{\sum_i K_{eq,i}z_i} \tag{20}$$

$$K_{eq,c} = \frac{1}{\frac{1}{K_{cf,c}} + \frac{1}{K_{cw,v}} + \frac{1}{K_c} + \frac{1}{K_{sc}}} \tag{21}$$

$$K_c = \frac{E_{s,c}{}^2\sqrt{b_{eff}d_{eff}}}{1.275E_r} \tag{22}$$

in which b_{eff} and d_{eff} are the effective width and depth of the contact between the slab and CFDST column, respectively.

2.2 Moment resistance

2.2.1 Joint under hogging moment

Guo *et al*. (2019b) proposes a reasonable component model to evaluate the moment resistance of semi-rigid composite connection to CFDST column, as depicted in Fig. 4 and expressed as follows

$$M_u = \sum_{i=1}^{m} F_{bo,i}(l_i - d_c) + \frac{F_{c,w}(d_c\text{-}t_f/2)}{2} + F_{c,f}d_c + F_{l,r}(l_{l,r} - d_c) + F_{u,r}(l_{u,r} - d_c) \tag{23}$$

$$d_c = \frac{\sum_i F_{i,r} + \sum_i F_{bo,i} - F_{c,j}}{f_{c,w}t_w} + \frac{t_f}{2} \tag{24}$$

$$F_{cw} = f_{y,w}t_w(d_c\text{-}t_f/2) \tag{25}$$

$$F_{l,r} + F_{u,r} = \min(\beta_v N_h f_{sc},\ f_y A_{l,r} + f_y A_{u,r}) \tag{26}$$

$$\frac{F_{l,r}}{F_{u,r}} = \frac{A_{l,r}}{A_{u,r}} \tag{27}$$

where $f_{y,w}$ and t_w are the strength and thickness of steel beam web, respectively; β_v is a coefficient considering the strength reduction in the hogging moment region according to GB50017 (2017); f_{sc} is the resistance of each shear connector.

$F_{bo,i}$ and $F_{c,f}$ are the resistances of bolt in tension and beam flange in compression, respectively, which are determined by various failure modes including end plate yielding, blind bolt failure, beam flange local buckling and column failure. For semi-rigid connections to square CFDST column, the strength of $K_{cf,c}$ and $K_{cw,s}$ for square CFDST column are not considered before. Here, $F_{bo,i}$ and $F_{c,f}$ in the case of column wall failure are determined by the load transfer mechanism (Hou *et al*. 2015).

$$F_{bo,i} = \pi f_{ck}\sqrt{\left\{[d_h + (1-\lambda)(D_o - 2t_o)]^2 - d_b^2\right\}(d_h{}^2 - d_b^2)} \tag{28}$$

$$F_{c,j} = 2f_{ck}\sqrt{[b_f + (1-\lambda)(D_o - 2t_o)][t_f + (1-\lambda)(D_o - 2t_o)]b_f t_f} \tag{29}$$

As a result, $F_{bo,i}$ and $F_{c,f}$ can be expressed as

$$F_{bo,i} = \min\begin{cases} \pi f_{ck}\sqrt{\left\{[d_h + (1-\lambda)(D_o - 2t_o)]^2 - d_b^2\right\}(d_h{}^2 - d_b^2)} \\ (5.5 - 0.021m_e + 0.017e)\cdot t_{ep}^2 \cdot f_{y,ep} \\ \frac{2A_{bo}\cdot f_{y,bo}}{\gamma_{bo}} \end{cases} \tag{30}$$

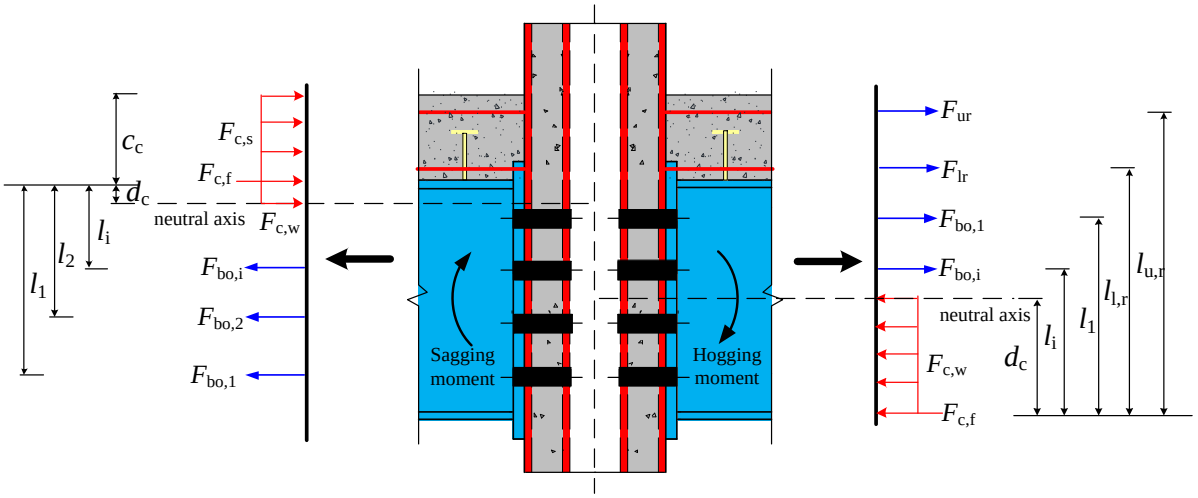

(I) Sagging moment (II) Hogging moment

(a) Flush end plate connection

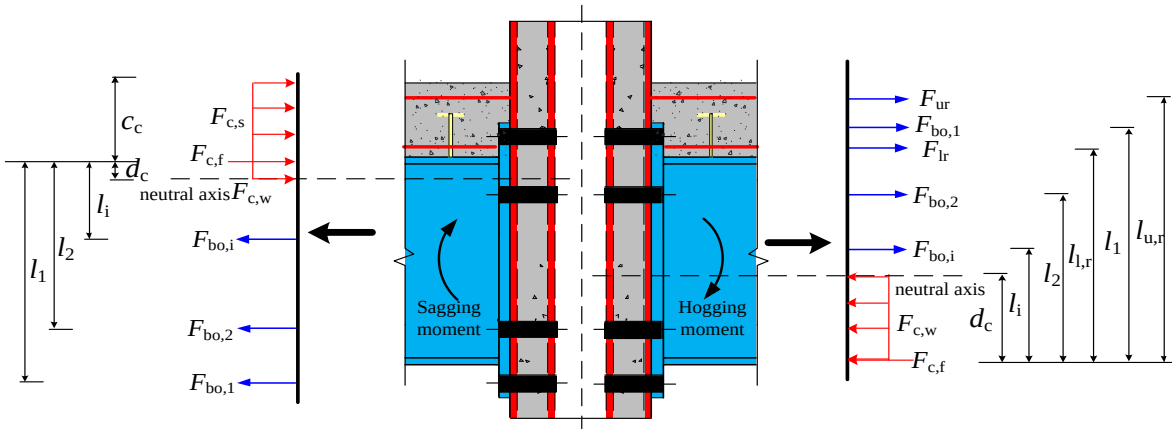

(I) Sagging moment (II) Hogging moment

(b) Extended end plate connection

Fig. 4 Component-based models to calculate the moment resistances of the connections

Table 1 Information of test specimens

Specimen	Outer tube $D_o \times t_{so}$ (mm)	Inner tube $D_i \times t_{si}$ (mm)	Beam section $h_b \times b_f \times t_w \times t_f$ (mm)	End plate type
SDSJ3-1	□ 250 × 8	□ 140 × 8	250 × 125 ×8 × 5.5	Flush end plate
SDSJ3-2	□ 250 × 8	□ 160 × 8	250 × 125 × 8 × 5.5	Flush end plate
SDSJ3-3	□ 250 × 8	□ 140 × 8	250 × 125 × 8 × 5.5	Extended end plate
SDSJ3-4	□ 250 × 8	□ 160 × 8	250 × 125 × 8 × 5.5	Extended end plate

$$F_{c,j}=\min\begin{cases}2f_{ck}\sqrt{[b_f+(1-\lambda)(D_o-2t_o)][t_f+(1-\lambda)(D_o-2t_o)]b_f t_f}\\ t_f b_f f_{y,f}\left(\dfrac{b_f}{t_f}\le 22\sqrt{\dfrac{235}{f_{y,f}}}\right)\\ 22t_f^2 f_{y,f}\sqrt{\dfrac{235}{f_{y,f}}}\left(\dfrac{b_f}{t_f}\ge 22\sqrt{\dfrac{235}{f_{y,f}}}\right)\end{cases} \tag{31}$$

in which f_{ck} is the characteristic strength of concrete; D_o and t_o are the width and thickness of outer steel tube, respectively.

2.2.2 Joint under sagging moment

Similarly, the component model of the connection under sagging moment is listed as follows

$$M_u = \sum_{i=1}^{m} F_{bo,i}(l_i - d_c) + \frac{F_{c,w} d_c}{2} + F_{c,f} d_c + F_{c,s}\left(\frac{c_c}{2} + d_c\right) \quad (32)$$

$$d_c = \frac{\sum_i F_{bo,i} - F_{c,j} - F_{c,s}}{f_{c,w} t_w} + \frac{t_f}{2} \quad (33)$$

$$F_{c,s} = \beta_v N_h f_{sc} + N_s f_{sc} \quad (34)$$

where c_c and N_s are the compressive depth of slab and number of the shear connector located in the sagging moment region, respectively.

3 Experimental validation

3.1 Test preparation

The joint model was selected based on a substructure of a multi-story composite frame. The configurations of the semi-rigid connections between the square CFDST columns and steel-concrete beam are shown in Fig. 5. Table 1 also lists basic information of the test connections. The blind bolts were anchored at the inner steel tube wall and provided a reliable connection between steel beams and CFDST columns. Furthermore, the blind bolts could be removed easily when the connection was damaged owing to serious earthquake loads.

In the test specimens, the steel tubes of the CFDST columns adopted square cross-sections. The outer steel tube was designed with a square hollow section (SHS) of 250 × 250 × 8 mm, while the SHS cross-section of inner steel tube was of 140 × 140 × 8 mm for specimens SDSJ3-1 and SDSJ3-3, and the SHS cross-section of inner steel tube was 160 × 160 × 8 mm for specimens SDSJ3-2 and SDSJ3-4. The height of the CFDST columns is determined as 1780 mm and the hollow ratio (χ) is expressed as follow

$$\chi = \frac{D_i}{D_o - 2t_o} \quad (34)$$

in which D_i refer to the outside width of the inner tube.

The hollow ratio (χ) of the CFDST columns for specimens SDSJ3-1 and SDSJ3-3 is 0.60; while the hollow ratio (χ) of the CFDST columns for specimens SDSJ3-2 and SDSJ3-4 is 0.68.

The steel beams of all specimens were H-shaped steel beam with a length of 1050mm. The end plate types are seen in the Fig. 5. Specimens SDSJ3-1 and SDSJ3-2 were connected by the flush end plates, while specimens SDSJ3-3 and SDSJ3-4 adopted extended end plates. The beam was attached to the CFDST column using blind bolts, as shown in Fig. 6. The blind bolt with the diameter of 20mm was tightened to the designed torque of 300N.m according to specification GB50017 (2017). Normal concrete was poured on the steel formwork of steel bar truss deck (SBTD) concrete slab with the thickness of 100 mm. The

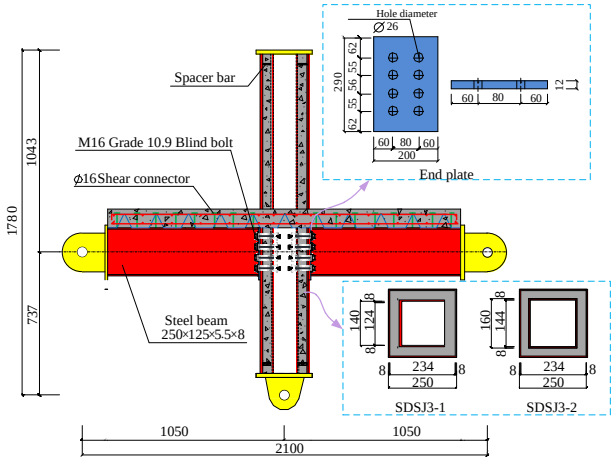

(a) Specimens SDSJ3-1 and SDSJ3-2

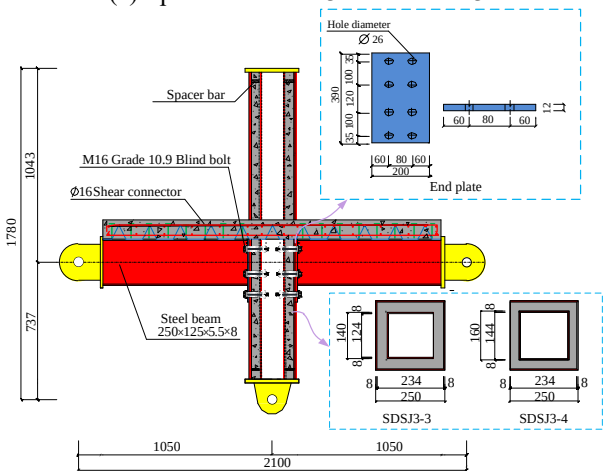

(b) Specimens SDSJ3-3 and SDSJ3-4

Fig. 5 Details of test specimens

details of SBTD concrete slab and the layout of reinforcement bars are illustrated in Fig. 5. Advantages of the SBTD concrete slabs have been certified by lots of engineering projects, such as simplifying the formwork construction, saving the assembling reinforcement and improving the integrality of the slabs.

The material test results of the steel for specimens are provided in Tables 2. The concrete cube compressive tests revealed that the elastic modulus and strength of the sandwiched concrete were 46.58N/mm^2 and 20534 N/mm^2, respectively, and those of the slab concrete were 35.58 N/mm^2 and 30534.1 N/mm^2, respectively.

Fig. 7 shows the photos and configurations of the experimental setup, respectively. For the typical interior column joint in the mid-story of frame, the inflection points of the beams and the columns are close to the mid-span under lateral cyclic forces. So, the pinned rolls were employed to connect the beam to the foundation beam, approximately imitating the real boundary condition in engineering practice. Thus, the lateral displacement-controlled load was exerted on the column end by the MTS actuator as the lateral seismic loading. Meanwhile, the axial load level (n) was chosen as 0.3 and defined as follows

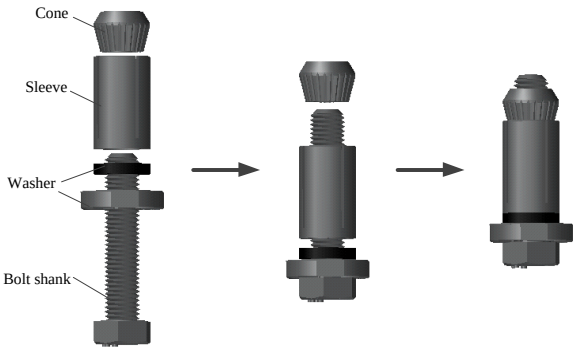

Fig. 6 Detail of blind bolts

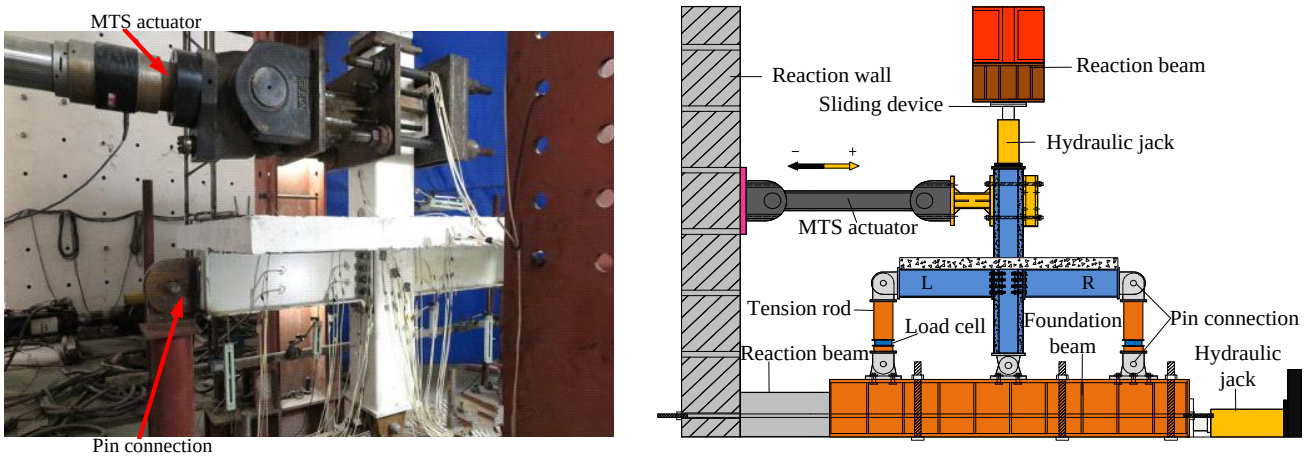

(a) Test photograph (b) Test set up

Fig. 7 Experimental setup
*+: Positive direction; -: Negative direction

Table 2 Material properties of steel

Steel components	Steel wall thickness (mm)	Yield stress f_y (N/mm^2)	Ultimate stress f_u (N/mm^2)	Young's modulus E_s (N/mm^2)	Elongation at fracture δ (%)
Steel tube	8	405	465	2.11×10^5	22.5
Steel beam flange	8	394	487	2.02×10^5	25.7
Steel beam web	5.5	446	568	2.24×10^5	30.2
End plate	12	400	551	1.98×10^5	20.7
Top chord rebar	10	351	525	1.87×10^5	24.7
Reinforcement bar-8	8	378	538	2.03×10^5	21.8
Bottom chord rebar	6	385	550	2.20×10^5	21.2

$$n = \frac{N_0}{N_u} \tag{36}$$

$$N_u = f_{scy} A_{sco} + f_{y,i} A_i \tag{37}$$

where N_0 is the axial load applied on the CFDST column; A_{sco} is the cross-section area including the outer steel tube and sandwiched concrete; f_{scy} is the combined compressive strength observed by Han *et al*. (2001). $f_{y,i}$ and A_i are the yield strength and cross-section area of inner tube, respectively.

The instruments were arranged to measure the force, deformation and stress of specimens in the tests. The lateral displacements and the corresponding loads were measured by the MTS actuator. The load cell was set at the support columns bottom to record the load of beam end. For each specimen, strain gauges were distributed on the main components of the specimens to record the strains, as shown in Fig. 8. Six linear variable displacement transducers

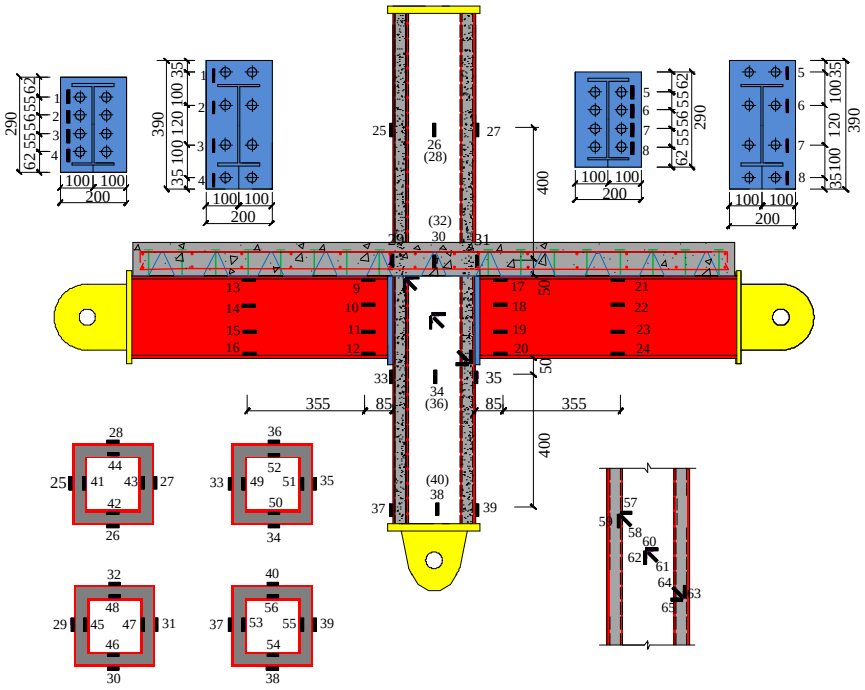

Fig. 8 Layout of strain gauges

(LVDTs) were used to measure the lateral displacements and the vertical displacements of composite beams. Three inclinometers were located on the column and the beams torecord the column and beam rotations, as shown in Fig. 9.

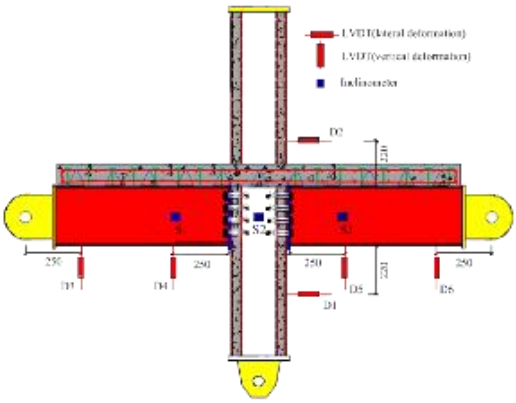

Fig. 9 Layout out of LVDTs and inclinometers

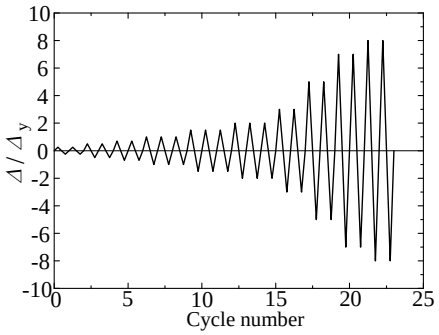

Fig. 10 Loading history

According to ATC-24 (1992), the loading history for all specimens is shown in Fig. 10, where the Δ_y equaled to 20 mm in the test and it was the estimated lateral yielding displacement based on a finite element analysis.

3.2 Failure modes

The specimens SDSJ3-1 and SDSJ3-2 were flush end plate joints to square CFDST columns with χ=0.60 and χ=0.68, respectively. The horizontal cracks on the middle of the slab top surface initiated at the cyclic level of 1 Δ_y, then penetrated through the slab along the length of the steel beam (main crack) with the increase of Δ. At the same time, a series of fine cracks were radiated especially along the main crack and periphery of the column outer tube on the top surface of the slab accompanied by the local crushing of concrete around the column walls. The end plates began to plastically deform with the slipping of the blind bolts at the cyclic level of 1.5 Δ_y. Failure of shear studs occurred at the cyclic level of 5Δ_y. Local buckling of the beam end flange was found at the cyclic level of 7 Δ_y. As concrete slab crushing around the column, buckling deformation of the beam flange was more severe with the increase of cyclic load. The test process of specimen SDSJ3-1 was terminated because of welding seam fracture on the beam flange, while the specimen SDSJ3-2 was terminated at the cyclic level of 8 Δ_y due to the large degradation of strength. Typical failure modes of specimens SDSJ3-1 and SDSJ3-2 are illustrated in Fig. 11.

The specimens SDSJ3-3 and SDSJ3-4 were extended end plate joints to square CFDST columns with χ=0.60 and χ=0.68, respectively. The phenomena observed in specimens SDSJ3-3 and SDSJ3-4 were similar to those of specimens SDSJ3-1 and SDSJ3-2, including slab top

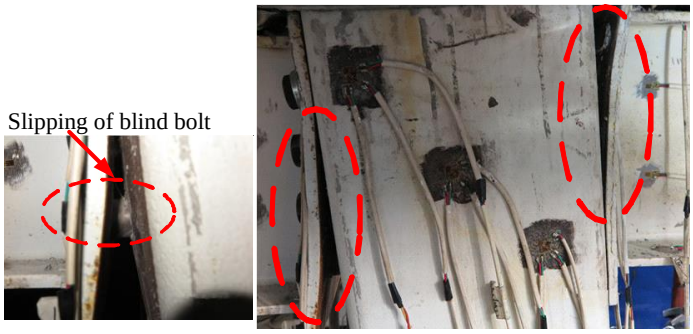

(a) Plastic deformation of end plate and slipping of blind bolt

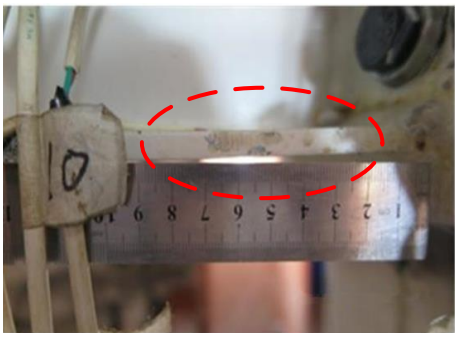

(b) Local buckling of beam flange

(c) Shear failure of shear studs in composite beam

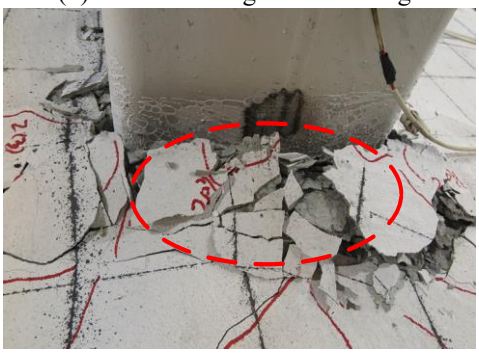

(d) Crushing of SBTD concrete slab

Fig. 11 Typical failure modes of flush end plate joint specimen

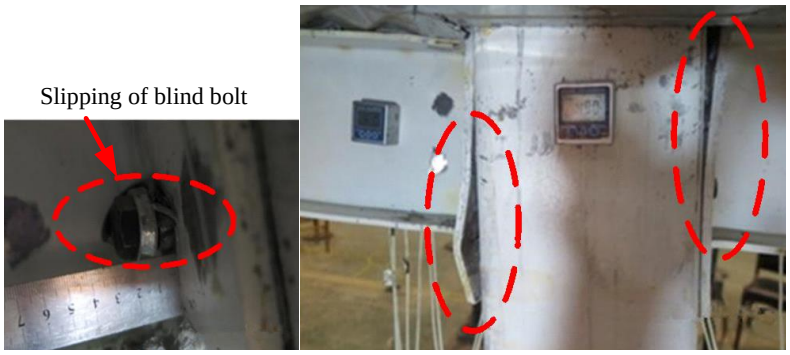

(a) Plastic Deformation of end plate and slipping of blind bolt

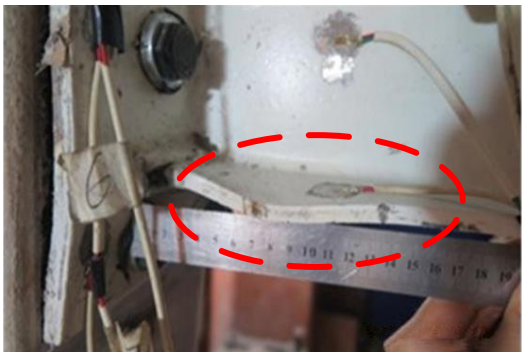

(b) Local buckling of beam flange

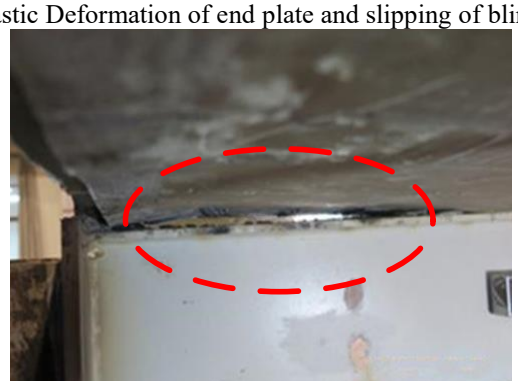

(c) Shear failure of shear studs in composite beam

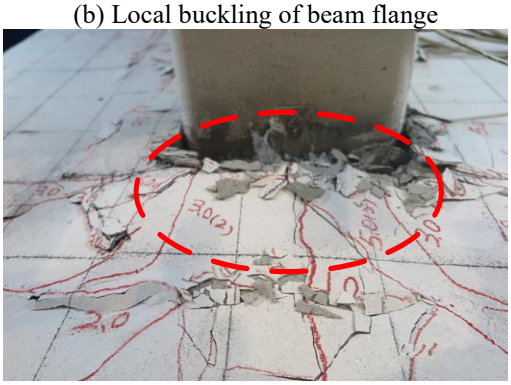

(d) Crushing of SBTD concrete slab

Fig. 12 Typical failure modes of extended end plate joint specimen

surface cracking (at the cyclic level of 1.5 Δ_y), extended end plates plastic deforming and blind bolt slipping (at the cyclic level of 1.5 Δ_y), shear failure of shear studs and concrete slab crushing (at the cyclic level of 5 Δ_y), and local buckling deformation (at the cyclic level of 7 Δ_y). Both two test specimens were terminated at the cyclic level of 8 Δ_y

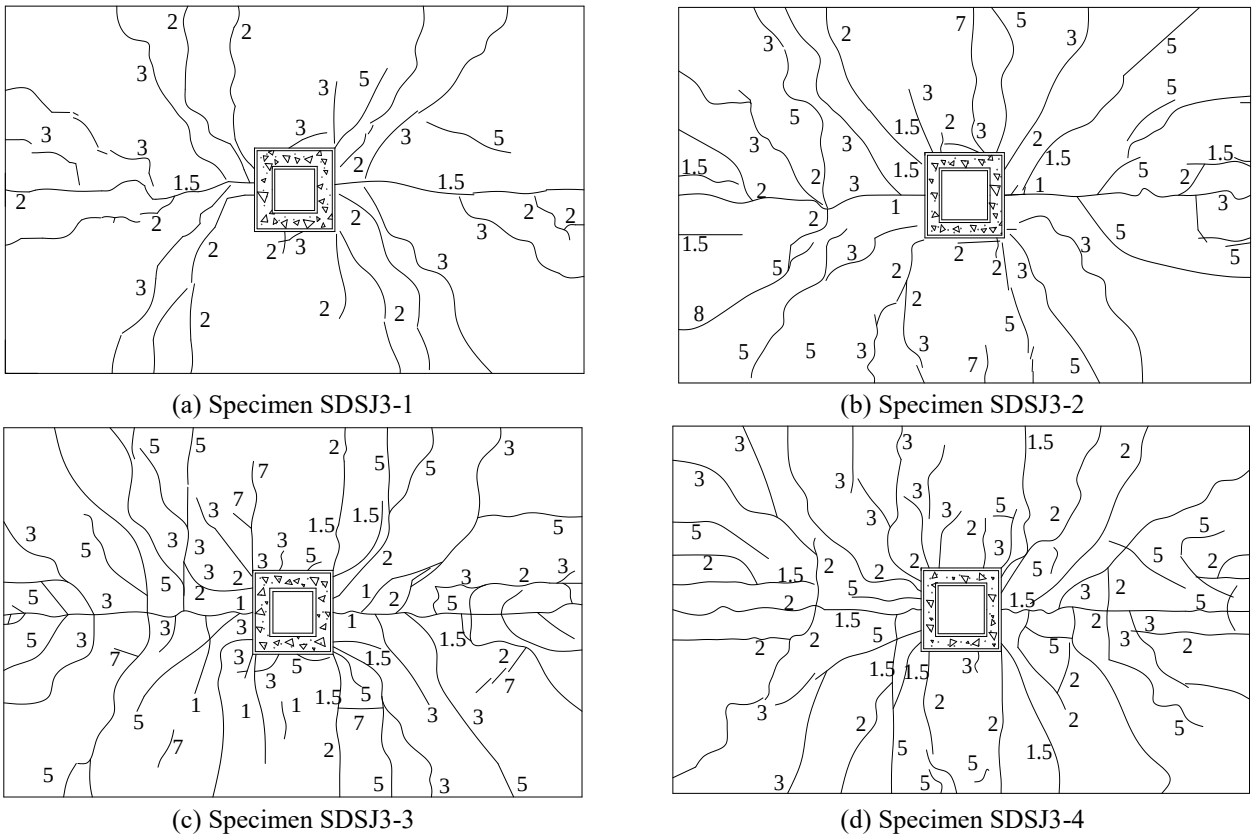

(a) Specimen SDSJ3-1 (b) Specimen SDSJ3-2

(c) Specimen SDSJ3-3 (d) Specimen SDSJ3-4

Fig. 13 Crack pattern of SBTD concrete slabs

when the strength degraded at 85% ultimate strength. Typical failure modes from the test are illustrated in Fig. 12.

For the joints with two types of the end plates, plastic deformation developed in flush end plate was more severe than that developed in extended end plate. Subsequently, the beam flange of extended end plate joint specimen exhibited more obvious local buckling deformation than that of flush end plate joint specimen. At the end of the test, slab concrete was partially extruded and serious spallation of the concrete around the column tube was observed. The effect of end plate type on cracking pattern of SBTD concrete slab is shown in Fig. 13. Compared with the composite joint with flush end plate, cracks of slab around the column were more serious for the composite joint with extended end plates under the same χ.

Moreover, for the composite joint with extended end plates, the slipping of blind bolts and local buckling of beam end were more serious than the composite joint with flush end plates under the same χ. For the semi-rigid composite joint to square CFDST column, the cracks on the slabs were mainly around the column, which was similar with the result from Guo *et al*. (2019).

3.3 Strain response of joint core

Fig. 14 displays the strains of inner and outer tubes near the joint core. It revealed that both the inner and outer tubes did not yield due to the beneficial of synergistic effect between the double steel tubes and the sandwiched concrete. More importantly, it was also found form the strain results that although the double tubes were in elastic stage, the column wall still appeared certain deformation.

Three strain rosettes numbered 57#-65# are attached on the outer tube to record the strains of column web, defined as 1-3# strain rosettes. Principle strain of each strain rosette was extracted as shown in Fig. 15. It could be observed that the principle strains of column web almost reached the yield strain of 1919 $\mu\varepsilon$ when reaching the ultimate moment capacity. In contrast with the experimental results, although no obvious deformation was noticed on the square CFDST column in the joint core, the column web still yielded. This might attribute to the composite action between the double steel tubes and sandwiched concrete.

As discussed above, although the strain results revealed that the CFDST column had not reached its yield strength and no obvious phenomenon was noticed on the CFDST column during the experiments, the CFDST column still actually exhibited certain deformation including the shear deformation of column web and compressive deformation of column web. For semi-rigid connections to CFST columns, the compressive deformation of column tube and shear deformation of column web could be ignored due to the concrete infill (Wang *et al*. 2009). However due to the hollow part of cross section existed in CFDST column, the compressive deformation of column tube and shear deformation of column web could not be neglected and

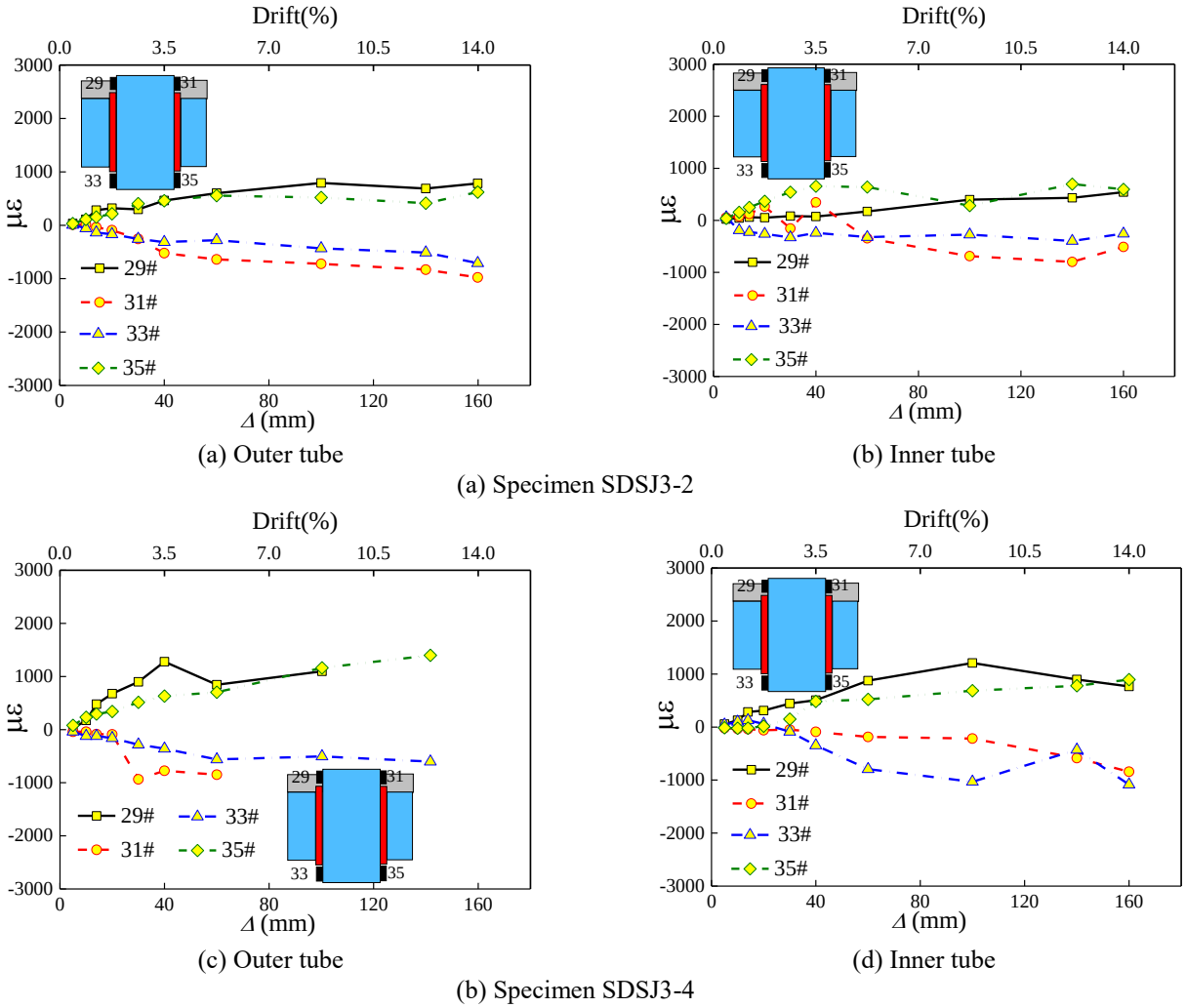

(a) Outer tube (b) Inner tube

(a) Specimen SDSJ3-2

(c) Outer tube (d) Inner tube

(b) Specimen SDSJ3-4

Fig. 14 Strains of column tube

would significantly affect the initial stiffness of the connection. It is verified that it is necessary to consider the stiffness and strength of $K_{cf,c}$ and $K_{cw,s}$ in the component model.

3.4 Moment (M) -rotation (θ_r) response

Relationships of connection moment (M) versus rotation (θ_r) for the blind bolted CFDST column composite joints are shown in Fig. 16. The connection moment could be calculated by the following expression

$$M = V_b \times L_0 \tag{38}$$

where, V_b is the vertical load recorded from the beam end by the load cells; and L_0 is the effective length measured from the right beam pin connection to the outer column face. The connection rotations (θ_r) were determined by the inclinometers

$$\theta_r = \theta_b - \theta_c \tag{39}$$

where θ_b and θ_c are the measured beam and column rotations, respectively.

Table 3 summarizes the moment capacities, rotation capacities, and initial stiffness of the composite joints, in which the yield moment and rotation were determined by Wang *et al*. (2016).

Comparisons on the M -θ_r curves of the semi-rigid composite joints are illustrated in Fig. 16. For the flush end plate joints, the ultimate moment capacity and initial stiffness of specimen SDSJ3-1 with χ=0.60 respectively improved by 9.56-10.34% and 6.97-10.55% compared with those of specimen SDSJ3-2 with χ=0.68. For the extended end plate composite joints, compared with specimen SDSJ3-4 with χ=0.68, the ultimate moment capacity and initial stiffness of specimen SDSJ3-3 with χ=0.60 respectively increased by 6.52-10.10% and 5.08-5.82%. The results indicated that the ultimate moment capacity and initial stiffness of the composite joint to square CFDST column improved with the decrease of χ. Moreover, the end plate type also affected the M -θ_r relationships of the composite joints. For the square CFDST column joints with χ=0.60, compared with specimen SDSJ3-1 with flush end plates, the ultimate moment capacity and initial stiffness of specimen SDSJ3-3 with extended end plates increased by

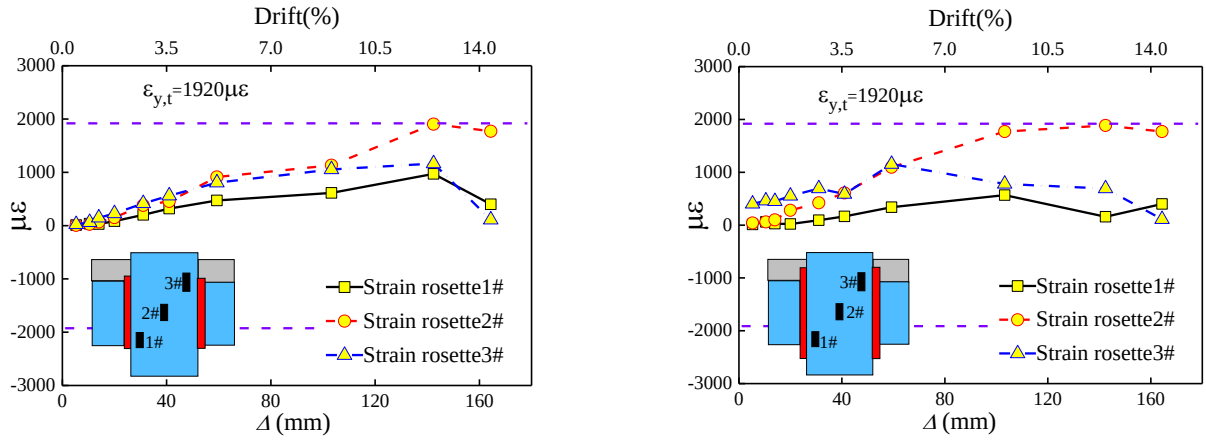

(a) Specimen SDSJ3-2 (b) Specimen SDSJ3-4

Fig. 15 Strains of CFDST column web

Table 3 Ultimate moment capacities, rotation capacities, and stiffness of connections

Specimen	Loading Direction	M_{yt}* (kN.m)	M_{ut} (kN.m)	M_{ft} (kN.m)	$\theta_{r,yt}$ (mrad)	$\theta_{r,ut}$ (mrad)	$\theta_{r,ft}$ (mrad)	$S_{j,ini}$ (kN.m/mard)
SDSJ3-1	+	155.63	182.35	155.00	26.67	46.32	60.99	11.42
	-	128.34	151.87	129.09	28.63	53.23	68.16	9.23
SDSJ3-2	+	132.09	166.44	144.47	31.68	46.65	72.39	10.33
	-	117.06	137.64	116.99	27.75	44.25	78.48	8.64
SDSJ3-3	+	159.68	199.85	183.13	24.03	66.10	77.23	15.10
	-	131.43	169.67	144.22	31.28	70.69	82.14	12.36
SDSJ3-4	+	145.68	181.51	155.29	28.38	72.65	85.74	14.37
	-	129.72	159.29	135.40	32.31	76.79	95.40	11.68

*M_{yt}: Yield moment; $\theta_{r,yt}$: Yield angular displacement; M_{ut}: Ultimate moment; $\theta_{r,ut}$: Ultimate angular displacement; M_{ft}=0.85 M_{ut}: Failure moment; $\theta_{r,ft}$: Failure angular displacement; $S_{j,ini}$: Initial stiffness

Table 4 Boundaries of connection classification according to EC3

Rigid classification	Rigid	$S_{j,ini} > K_b EI_b/L_b$
	Semi-rigid	$0.5\ EI_b/L_b \le S_{j,ini} \le K_b EI_b/L_b$
	Nominally pinned	$S_{j,ini} < 0.5\ EI_b/L_b$
Strength classification	Full-strength	$M_u^* > M_{bp}$
	Partial strength	$0.25\ M_{bp} \le M_u \le M_{bp}$
	Nominally pinned	$M_u \le 0.25\ M_{bp}$

* M_u: Ultimate moment capacity; M_{bp}: Design plastic moment resistance of the steel beam

9.60-11.72% and 32.22-33.91%, respectively. For the square CFDST column joints with χ=0.68, increases of the ultimate moment capacity and initial stiffness of specimen SDSJ3-4 with extended end plate were respectively 9.05-15.73% and 35.19-39.11% compared with specimen SDSJ3-2 with flush end plates. It declared that χ had a limited influence on the mechanical behavior of the connections, while the end plate type had a convincing effect on the initial stiffness and had a moderate effect on the mechanical behavior of the connections due to the failure of shear studs.

Connections could be classified as rigid, nominally pinned, and semi-rigid through their stiffness, or defined as full-strength, nominally pinned, as well as partial strength by their strength. The boundaries of stiffness and moment capacity to classify the type of connection according to EC3 (2005) are listed in Table 4. Fig. 17 presents the classification results of the CFDST column joints. The non-dimensional coefficients $\overline{\theta}$ and $\overline{M}$ are expressed as follows

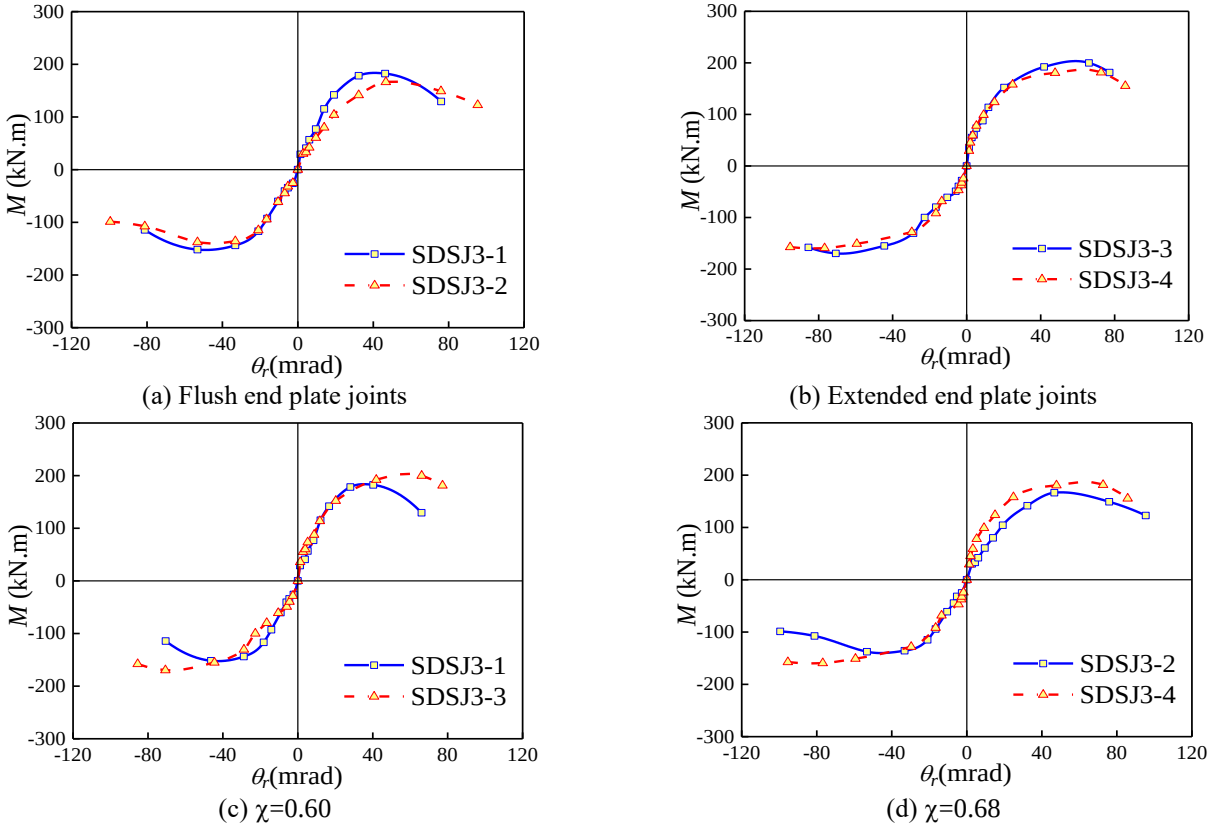

(a) Flush end plate joints (b) Extended end plate joints

(c) χ=0.60 (d) χ=0.68

Fig. 16 Moment (M) versus rotation (θ_r) relationship of specimens

Table 5 Comparison between predicted and experimental results

Specimen		$M_{y,t}$ (kN.m)	$M_{y,p}$ (kN.m)	$M_{y,p}/M_{y,t}$	$S_{j,ini,t}$ (kN.m/mrad)	$S_{j,ini,p}$ (kN.m/mrad)	$S_{j,ini,p}/S_{j,ini,t}$
SDSJ 3-1	+*	155.63	137.43	0.88	11.42	9.96	0.87
	-	128.34	131.65	1.03	9.23	8.57	0.93
SDSJ 3-2	+	132.09	137.43	1.04	10.33	9.73	0.94
	-	117.06	131.65	1.12	8.64	8.24	0.95
SDSJ 3-3	+	159.68	163.17	1.02	15.10	11.21	0.94
	-	131.43	145.01	1.10	12.36	13.69	0.95
SDSJ 3-4	+	145.68	163.17	1.12	14.37	11.78	0.95
	-	129.72	145.01	1.12	11.68	14.13	0.96

*+: Sagging moment; -: Hogging moment; t: Experimental results; p: Predicted result

$$\overline{M} = M / M_{bp} \tag{40}$$

$$\overline{\theta} = \frac{\theta_r}{M_{bp}} \frac{EI_b}{L_b} \tag{41}$$

It indicated that all test joints were classified as semi-rigid and partial strength connections under both sagging and hogging moments.

Table 5 presents the comparison results between the component model and the experimental results. It revealed that the calculated results from the component model coincided well with the test results, which confirmed that it was necessary to consider the stiffness and strength of $K_{cf,c}$

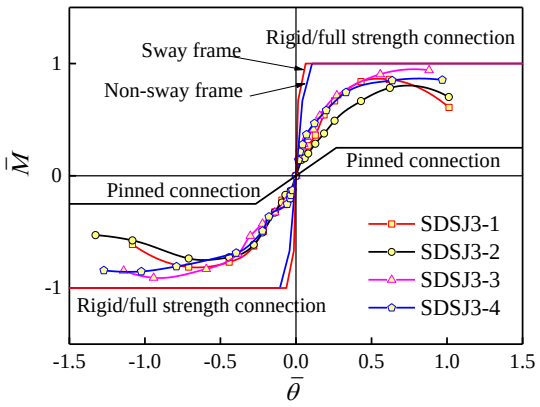

Fig. 17 Classification of test specimens

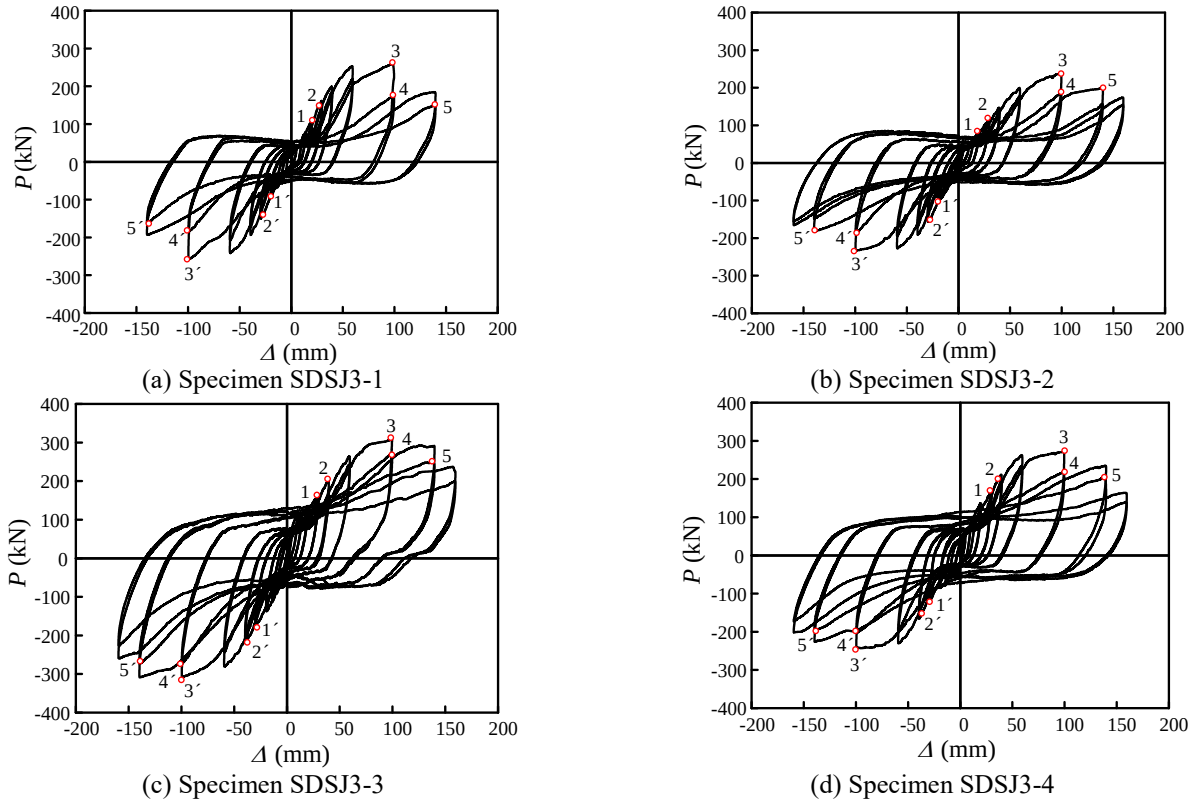

(a) Specimen SDSJ3-1 (b) Specimen SDSJ3-2

(c) Specimen SDSJ3-3 (d) Specimen SDSJ3-4

Fig. 18 Overall behavior curves of the specimens

*1(1'): Slab's initial cracking; 2(2'): Yielding point; 3(3'): Ultimate strength; 4(4'): Failure of shear stud; 5(5'): Local buckling of beam end

and $K_{cw,s}$ for semi-rigid connections to CFDST columns in the component model. Further, the proposed component model was also validated to be capable of predicting the mechanical performance of the semi-rigid connection.

4. Seismic performance

4.1 P-Δ hysteretic curves

Load-displacement (P-Δ) relationships are illustrated in Fig. 18. The horizontal load (P) of column end versus the lateral displacement (Δ) of loading position was recorded by MTS actuator.

In Fig. 18, obvious pinching effect could be observed on the hysteretic curves for each specimen. This might contribute by the crushing damage of slab concrete, loss of bolt anchorage for blind bolt slipping and the plastic deformation of end plates and steel beams. As shear failure of shear studs and local buckling of beam end, remarkable strength and rigidity degradation occurred for all specimens when the lateral displacement $\Delta \geq 5\ \Delta_y$. Generally, the comparison confirmed that the semi-rigid joints to square CFDST columns had excellent hysteretic behavior and dissipation capacities.

4.2 Rotation ability and ductility

Ductility coefficient (μ_θ) and rotation ability were also employed to assess the seismic performance of the semi rigid joints. Ductility coefficient (μ_θ) could be defined as

$$\mu_\theta = \frac{\theta_{ft}}{\theta_{yt}} \tag{42}$$

in which θ_{ft} and θ_{yt} are the failure angular displacement and the yield angular displacement taken from the moment (M)-rotation (θ_r) envelope curves, respectively.

Values of μ were respectively 2.29, 2.28, 3.21, and 3.02 for specimens SDSJ3-1, SDSJ3-2, SDSJ3-3, and SDSJ3-4 under sagging moment, and were respectively 2.38, 2.82, 2.63 and 2.95 for specimens SDSJ3-1, SDSJ3-2, SDSJ 3-3 and SDSJ3-4 under hogging moment.

It demonstrated that both the column hollow ratio and end plate type had limited effects on the ductility of the test specimens. This could be explained by that fracture of shear studs occurred for all specimens. It also concluded that the rotational abilities of the specimens under hogging moment were higher than those under sagging moment owing to that the influence of concrete slab was more significant under sagging moment. Moreover, the joints to square CFDST columns possessed favorable rotation capacities and could meet the ductility requirement of FEMA-350 (2000).

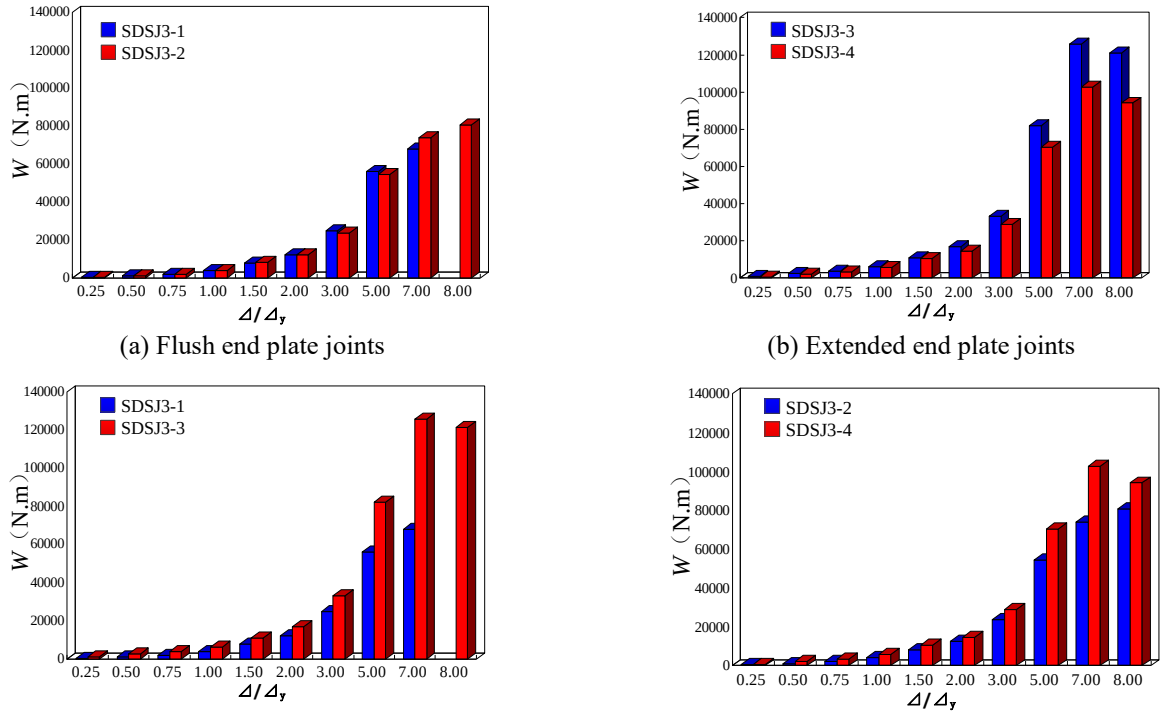

(a) Flush end plate joints

(b) Extended end plate joints

(c) χ=0.60

(d) χ=0.68

Fig. 19 Comparison on energy dissipation of test specimens

4.3 Energy dissipation

The energy dissipation capacity of the test joint was evaluated by energy dissipation coefficient (W), which was the accumulated area of load-displacement (P-Δ) hysteretic loops for each displacement level. The comparisons of W for the test joint are illustrated in Fig. 19. From the test results, it could be found that values of W increased with the increase of lateral displacement for specimens SDSJ3-1 and SDSJ3-2, while W of specimens SDSJ3-3 and SDSJ3-4 increased when $\Delta/\Delta_y \leq 7$ and then decreased with increase of displacement level. It could be explained for the serious local buckling deformation on the beam end flange of specimens SDSJ3-3 and SDSJ3-4.

The energy dissipation capacity of the semi rigid joint with extended end plates was greater than that of the semi rigid joint with flush end plates under the same χ. The joints with low χ possessed larger energy dissipation capacities under the same end plate type. However, specimen SDSJ3-1 with χ=0.60 failed at the cyclic level of 7 Δ_y due to welding seam fracture on the beam flange which caused the lower energy dissipation capacity of specimen SDSJ3-1 than specimen SDSJ3-2 with χ=0.68.

5 Conclusions

The analytical and experimental investigation in this paper could provide following conclusions:

- Typical failure modes of the semi-rigid composite joints between the square CFDST columns and steel-composite beams could be concluded as follows: SBTD concrete slab cracking; plastic deformation of end plate; slipping of the blind bolt; local buckling of the beam flange; failure of shear studs in composite beam. However, compared with CFST column joint, there was no fracture and buckling on CFDST column wall in connection region.
- Compared with the semi rigid joint with flush end plates, the semi rigid joint with extended end plates performed relatively high strength and initial stiffness under the same χ. The ultimate strength and initial stiffness of the CFDST columns joint with χ=0.60 were larger than those of the CFDST column joint with χ=0.68 under the same end plate type. Moreover, the composite joints to square CFDST columns could be classified as semi-rigid connections under both sagging and hogging moments.
- This type of joint performed excellent seismic behavior in terms of good rotation abilities, ductility and energy dissipation capacities. Their rotation capacities exceeded 30mrad and satisfied the ductility requirement of the structure in the earthquake-resistance design. The energy dissipation capacity of the semi-rigid joint to square CFDST column with flush end plates was inferior to that of the semi-rigid joint to square CFDST column with extended end plate joint under the same χ, while the energy dissipation capacity of the semi rigid joint to square CFDST column with joint improved with the decrease of χ for the joint with the same end plate type.
- A component model was established to assert the initial stiffness of the semi rigid joint between the steel-concrete composite beam and square CFDST column,

focusing on the strength and stiffness of $K_{cf,c}$ and $K_{cw,s}$ for CFDST column. The predicted results were verified by the experimental results, indicating that the proposed component model was appropriate to predict the mechanical performance of this type of connection.

Acknowledgments

The experiments conducted in this paper is supported by National Natural Science Foundation Project 51478158 and 51178156. Also, the staff in Anhui Civil Engineering Structures and Materials Laboratory is highly appreciated.

References

Agheshlui, H., Goldsworthy, H., Gad, E. and Mirza, O. (2017), "Anchored blind bolted composite connection to a concrete filled steel tubular column", *Steel Compos. Struct*., **23**(1), 115-130. https://doi.org/10.12989/scs.2017.23.1.115.

Aribert, J.M. (1996), "Influence of slip of the shear connection on composite joint behavior", *Proceedings of the 3rd International Workshop on Connections in Steel Structures*, Pergamon, Trento, October.

ATC-24 (1992), Guidelines for cyclic seismic testing of components of steel structures, Applied Technology Council; Redwood City, America.

CEB-FIP Model Code (1990), Design Code, Committee Euro-International du Beton, Lausanne, Thomas Telford Services Ltd; London, England.

Chen, Y., Feng, R. and Ruan, X.F. (2016), "Behaviour of steel-concrete-steel SHS X-joints under compression", *J. Constr. Steel Res*., **122**, 469-487. https://doi.org/10.1016/j.jcsr.2016.04.006.

Du, G.F., Bie, X.M., Li, Z. and Guan, W.Q. (2005), "Elastoplastic behavior of panel zone in steel beam-to-concrete filled steel tube column moment connections", *J. Struct. Eng*., **131**(12), 1841-1853. https://doi.org/10.1061/(ASCE)0733-9445(2005)131:12(1841).

EC 3 (2005), Design of steel structures-Part 1-8: Design of joints, European Committee for Standardisation (CEN); Brussels, Belgium.

EC 4 (2004), Design of composite steel and concrete structures-Part 1-1: Composite joints in frames for buildings. European Committee for Standardisation (CEN); Brussels, Belgium.

Farahi, M., Heidarpour, A., Zhao, X.L. and Al-Mahaidi, R. (2016), "Compressive behaviour of concrete-filled double-skin sections consisting of corrugated plates", *Eng. Struct*., **111**, 467-477. https://doi.org/10.1016/j.engstruct.2015.12.012.

FEMA-350 (2000), Recommended seismic design for new steel moment-frame buildings, Federal Emergency Management Agency; Washington DC, America.

GB50017 (2017), Code for design of steel structures, Ministry of Housing and Urban-Rural Development; Beijing: China.

Guo, L., Wang, J.F., Wang, W.Q. and Duan, M.J. (2019b), "Seismic evaluation and calculation models of CFDST column blind bolted to composite beam joints with partial shear interaction", *Eng. Struct*., **196**, 109269. https://doi.org/10.1016/j.engstruct.2019.06.005.

Guo, L., Wang, J.F., Wu, S.C. and Zhong, L.P. (2019a), "Experimental investigation and analytical modelling of blind bolted flush or extended end plate connections to circular CFDST columns", *Eng. Struct*., **192**, 233-253. https://doi.org/10.1016/j.engstruct.2019.04.053.

Han, L.H., Tao, Z., Huang, H. and Zhao, X.L. (2004), "Concrete-filled double skin (SHS outer and CHS inner) steel tubular beam-columns", *Thin-Wall. Struct*., **42**(9), 1329-1355. https://doi.org/10.1016/j.tws.2004.03.017.

Han, L.H., Zhao X.L. and Tao, Z. (2001) "Tests and mechanics model of concrete-filled SHS stub columns, columns and beam-columns" *Steel Compos. Struct*., **1**, 51-74. https://doi.org/10.1296/SCS2001.01.01.04.

Hou, C. and Han, L.H. (2017), "Analytical behaviour of CFDST chord to CHS brace composite K-joints", *J. Constr. Steel Res*., **128**, 618-632. https://doi.org/10.1016/j.jcsr.2016.09.027.

Hou, C., Han, L.H. and Zhao, X.L. (2015), "Behaviour of circular concrete filled double skin tubes subjected to local bearing force", *Thin-Wall. Struct*., **93**, 36-53. https://doi.org/10.1016/j.tws.2015.03.004.

Huang, H., Han, L.H. and Zhao X.L. (2013), "Investigation on concrete filled double skin steel tubes (CFDSTs) under pure torsion", *J. Constr. Steel Res*., **90**(5), 221-234. https://doi.org/10.1016/j.jcsr.2013.07.035.

Liu, Y., Chuquitaype, M. and Elghazouli, A.Y. (2012), "Response and component characterisation of semi-rigid connections to tubular columns under axial loads", *Eng. Struct*., **41**, 510-532. https://doi.org/10.1016/j.engstruct.2012.03.061.

Mirza, O. and Brain, Uy. (2011), "Behaviour of composite beam-column flush end-plate connections subjected to low-probability, high-consequence loading", *Eng. Struct*., **33**(2), 647-62. https://doi.org/10.1016/j.engstruct.2010.11.024.

Theodoros, P. and Walid, T. (2015), "A component method model for blind-bolts with headed anchors in tension", *Steel Compos. Struct*., **18**, 1305-1330. https://doi.org/10.12989/scs.2015.18.5.1305.

Wang, J.F., Guo, L., Guo, X. and Ding, Z.D. (2019), "Seismic response investigation on CFDST column to steel beam blind-bolted connections", *J. Constr. Steel Res*., **161**, 137-153. https://doi.org/10.1016/j.jcsr.2019.04.030.

Wang, J.F., Han, L.H. and Brian, Uy. (2009), "Behaviour of flush end plate joints to concrete-filled steel tubular columns", *J. Constr. Steel Res*., **65**, 925-939. https://doi.org/10.1016/j.jcsr.2008.10.010.

Wang, Z.B., Tao, Z., Li, D.S. and Han, L.H. (2016), "Cyclic behaviour of novel blind bolted joints with different stiffening elements", *Thin-Wall. Struct*., **101**, 157-168. https://doi.org/10.1016/j.tws.2016.01.007.

Wei, S., Mau, S.T., Vipulanandan, C. and Mantrala, S.K. (1995), "Performance of new sandwich tube under axial loading: experiment", *J. Struct. Eng*., **121**(12), 1806-1814. https://doi.org/10.1061/(ASCE)0733-9445(1995)121:12(1806).

Yang, Y.F., Hou, C., Meng, C.Y. and Han, L.H. (2015), "Investigation on square concrete filled double-skin steel tube (CFDST) subjected to local bearing force: Experiments", *Thin-Wall. Struct*., **94**, 394-409. https://doi.org/10.1016/j.tws.2015.04.026.

Zhou, F. and Xu, W. (2016), "Cyclic loading tests on concrete-filled double-skin (SHS outer and CHS inner) stainless steel tubular beam-columns", *Eng. Struct*., **127**, 304-318. https://doi.org/10.1016/j.engstruct.2016.09.003.

BU